

## Highlights

### **Breccia and basalt classification of thin sections of Apollo rocks with deep learning**

Freja Thoresen, Aidan Cowley, Romeo Haak, Jonas Lewe, Clara Moriceau, Piotr Knapczyk, Victoria S. Engelschiøn

- State-of-the-art machine learning techniques and analyses applied to a comprehensive dataset of lunar rock thin section images.
- Contrastive learning on lunar rock thin sections to capture the underlying features of the images.
- Binary classifier of breccia/basalt rock textures with transfer learning from Inception-ResNet-v2 achieves an accuracy of 98.44

# Breccia and basalt classification of thin sections of Apollo rocks with deep learning

Freja Thoresen<sup>a</sup>, Aidan Cowley<sup>b</sup>, Romeo Haak<sup>b</sup>, Jonas Lewe<sup>b</sup>, Clara Moriceau<sup>b</sup>, Piotr Knapczyk<sup>b</sup>, Victoria S. Engelschiøn<sup>b,c</sup>

<sup>a</sup>*Directorate of Human and Robotics Exploration, European Space Agency (ESA), European Space Research and Technology Centre (ESTEC), Noordwijk, Netherlands*

<sup>b</sup>*Directorate of Human and Robotics Exploration, European Space Agency (ESA), European Astronaut Centre (EAC), Cologne, Germany*

<sup>c</sup>*The Natural History Museum, University of Oslo, Oslo, Norway*

---

## Abstract

Human exploration of the moon is expected to resume in the next decade, following the last such activities in the Apollo programme time. One of the major objectives of returning to the Moon is to continue retrieving geological samples, with a focus on collecting high-quality specimens to maximize scientific return. Tools that assist astronauts in making informed decisions about sample collection activities can maximize the scientific value of future lunar missions. A lunar rock classifier is a tool that can potentially provide the necessary information for astronauts to analyze lunar rock samples, allowing them to augment in-situ value identification of samples. Towards demonstrating the value of such a tool, in this paper, we introduce a framework for classifying rock types in thin sections of lunar rocks. We leverage the vast collection of petrographic thin-section images from the Apollo missions, captured under plane-polarized light (PPL), cross-polarised light (XPL), and reflected light at varying magnifications. Advanced machine learning methods, including contrastive learning, are applied to analyze these images and extract meaningful features. The contrastive learning approach fine-tunes a pre-trained Inception-Resnet-v2 network with the SimCLR loss function. The fine-tuned Inception-Resnet-v2 network can then extract essential features effectively from the thin-section images of Apollo rocks. A simple binary classifier is trained using transfer learning from the fine-tuned Inception-ResNet-v2 to 98.44% ( $\pm 1.47$ ) accuracy in separating breccias from basalts.

*Keywords:* Thin sections of rock, Apollo lunar samples, deep neural networks, binary classifier, contrastive learning

---

## 1. Introduction

The analysis of lunar samples is crucial to understanding the formation, evolution, and resource potential of the Moon [1]. Hence, rock sample collection is one of the important scientific objectives of returning to the Moon. Information on rock type or specific mineralogy may help study the lunar geology and can be used for decision-making, e.g., if the material is suitable for a particular experiment or return to Earth [2].

The vast collection of Apollo rocks has been studied extensively. A common geological method is petrographic thin sections, where rock specimens are polished to a thickness of 30  $\mu\text{m}$  [3, 4, 5]. These are then examined in an optical microscope by rotation under differing light conditions to determine the minerals and textures within the rocks, known as petrography [6]. While effective, this method is time-consuming and requires expertise; subsequently, there is a need for automated or semi-automated systems for analyzing lunar rocks in order to maximize the scientific output of lunar missions. In recent years, machine learning has shown to be a powerful tool for automating the analysis of thin-section images [7]. Deep learning, especially convolutional neural networks (CNN), has impressive performance in image classification and segmentation tasks [8, 9].

This study introduces a method for classifying rock textures in thin sections of lunar breccias and basalts and establishes a framework for additional analysis, including segmentation and clustering. It aims to aid in developing tools that help astronauts analyze thin sections of lunar rock, such as identifying rocks of particular interest. This information can help guide further collection efforts, allowing targeted sampling of promising sites and maximizing the scientific returns of lunar missions for analysis back on Earth, in addition to providing impetus for the development of IVA (in-vehicle activity) thin-section/microscopy capabilities for future lunar astronauts.

### 1.1. Building Blocks of the Moon

The Moon mainly consists of the igneous rocks anorthosite and basalt, and breccias, which are aggregates of broken rock fragments cemented together. Anorthosite is a calcium-rich rock that largely makes up the ancient crust of the Moon [10].

Lunar basalts are the product of the partial melting of the lunar mantle, primarily found in the Mare regions of the Moon [3]. They are low in silica and contain more iron and less total silicon ( $\text{SiO}_2$ ) than terrestrial basalts.

Lunar basalts typically comprise pyroxene, plagioclase, olivine, and metal oxides such as ilmenite, armalcolite, and spinel [3].

Breccias are cemented rocks formed by impacts and may contain fragments of both anorthosites and basalts [11]. They are composite rocks composed of fragments of older rocks broken apart, mixed, and then bound together [3]. These rock fragments are known as clasts, and they are held together by a matrix, which can be composed of finer fragments of the same materials or a different rock type [3]. Lunar breccias were formed by the heat and pressure generated by impacts, and most were formed in the lunar highlands [3].

### *1.2. Petrological Analysis of Thin Sections of Lunar Rock*

As mentioned, Apollo rocks have been studied extensively, and over the years, a collection of labeled thin-section images from the Apollo missions has been created [12, 13, 14, 15, 16, 17, 18]. The thin sections are made by cutting, smoothing, and polishing rocks to a  $30\mu\text{m}$  thickness and are typically imaged under various lighting conditions (plane-polarized light (PPL), cross-polarized light (XPL), and reflected light) [4]. The number of thin sections per sample varies significantly, ranging from 2 to 70, depending on the extent of prior studies. Additionally, each thin section has multiple images, often at varying magnifications (2.5-10x) and focusing on different regions of the section.

While thin sections of lunar rocks were created when they were returned and analyzed on Earth, an interesting prospect is to make the thin sections in a lunar laboratory. In [19], designs for an automated rock thin section device are suggested, which may efficiently cut future rock samples in a space environment. In Figure 1, a concept of a semi-automatic machine is shown, which was developed in 1965. Development of tools and payloads to support astronauts with in-situ science analysis capability represents a new paradigm for exploration and will be increasingly important in future missions beyond LEO - ultimately, a level of laboratory capability will be required as Moon and even Mars missions make terrestrial return logistics challenging.

### *1.3. Analysis of thin sections of lunar rock using machine learning techniques*

Previous studies have utilized machine learning techniques to cluster, classify, or segment thin sections of rocks. For instance, efforts have been

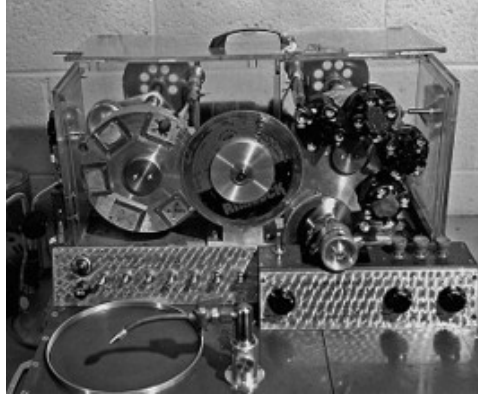


Figure 1: In 1965, the United States Geological Survey (USGS) developed a prototype for a semi-automatic machine to cut and prepare thin sections of rocks [20]. This innovative device was specifically designed for the Apollo Applications Program and Advanced Lunar Programs Groups, aiming to streamline the analysis of lunar samples.

made to segment photomosaics of thin sections of carbonate rocks originating from sidewall core samples of oil wells [21]. The photomosaics were segmented into different minerals (calcite, dolomite, quartz, opaque minerals, clays, and others) and porosities, using a model with discrete convolutional filters followed by artificial neural networks and random forest classifiers [21]. A different segmentation approach involves using images of six angles of single-polarization and orthogonal polarizations to segment petrographic thin-sections into mineral components [22]. The process includes manually labeling the samples and training a Mask R-CNN network with transfer learning from ResNet34 [22]. The approach segments petrographic thin section components in tight oil reservoirs, demonstrating improvements in accuracy and speed [22]. In [23], a method for classifying thin-section images using residual networks (ResNet50 and ResNet101) is introduced in order to achieve automatic feature extraction and classification based on image size. Experimental results show that the two network structures achieve high accuracy (90.24% and 91.63%) on the test set, demonstrating the effectiveness of the proposed method for efficient and accurate thin-section classification [23]. Another approach uses CNNs to classify 13 rock types [24]. A concatenated Convolutional Neural Network is used to classify rocks based on photographed thin sections in PPL and XPL lighting conditions. Five-fold cross-validation shows that the method proposed provides an overall accuracy of 89.97% and a Kappa coefficient of 0.86 [24].

In conclusion, the sources showcase the versatility of machine learning

techniques in analyzing petrographic thin-sections. Segmentation tasks focus on classifying individual pixels within an image, while classification approaches aim to categorize entire images based on features like mineral composition or grain size.

## 2. Data

Two databases are used in this study: The NASA PDS database [25] and the Lunar Institute Data [26]. The NASA PDS database contains digitally scanned versions of the original film photographs of rock, soil, and core samples collected from the lunar surface during the Apollo missions. The images are captured under three lighting conditions (plane-polarized light (PPL), cross-polarized light (XPL), and reflected light), as seen in Figure 2. While there are images of different views of the Apollo rock samples on the data note, in this analysis, only the thin sections of rock images were considered. Furthermore, the thin sections of Apollo rocks exist in different resolutions and formats on the PDS3 note, where in this analysis, the full-resolution JPEG format was chosen as the ideal candidate in a trade-off of storage size and resolution. In addition to the images, the label files were also used in the analysis, which contains information on samples and photo descriptions. There are 365 samples in the dataset, with 5203 images of thin sections of the rock images, as one rock sample can have several images.

Like the NASA PDS database, the Lunar Institute Data also contains digitally scanned versions of original film photographs of rock, soil, and core samples collected from the Apollo missions. Selecting thin sections of Apollo rocks resulted in 605 samples and 17066 images. Samples 10072A and 10072 were excluded since no labeled data was found.

While there are overlapping samples between the two datasets, each data set often contains unique information, such as interpretations of the mineralogies of the thin-section images. The information from both sources was integrated, and duplicate information or pictures were removed from the collective dataset. Further details on the samples were retrieved from the Lunar Sample and Photo Catalog Curator [27] to fill in gaps of knowledge where needed. Images with mislabelling, manual markings, or where the thin section occupied less than 60% of the image area were excluded from the dataset. Black borders and artifacts of the scanning process were cropped from images in the LPI dataset. Lastly, as sample 12003, exclusive to the PDS dataset, had multiple images, the erroneous reference to image s70-48868 was removed from the combined dataset. The overall distribution of data is in Table 1.

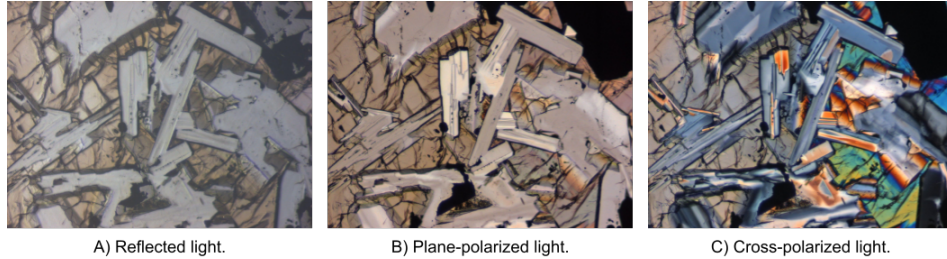


Figure 2: Example of a thin section under different polarized light conditions: Reflected light, plane-polarized light, and cross-polarised light.

Category	Samples	Images
Basalt	187	4769
Breccia	326	8470
Total	513	13239

Table 1: Distribution of samples and images by rock texture category.

### 2.1. Data Preprocessing

In the data preprocessing, the dataset is split into training, validation, and a test set. For each split, images of the same sample end up in the same set. The dataset is split for training purposes in the following way: 60% training, 20% validation, and 20% testing.

The images are resized to 299x299x3, and the pixel color values of the images are normalized. The data is augmented by a layer in the training of the network, with augmentations of random vertical/horizontal rotations, random zoom, brightness, saturation, hue, and contrast. The augmentations artificially create more data, making the network more robust to small perturbations, thus preventing overfitting [28]. An example of augmentations of an image of a thin section of lunar rock is in Figure 3.

As seen in Table 1, the dataset is imbalanced. Therefore, class frequencies are calculated to generate class weights to counteract potential problems arising from the imbalance. During the training, the class weights are then applied to the dataset, making the less abundant class more relevant, thus improving the imbalance.

## 3. Network Architecture

The methodology employed in this paper will leverage contrastive learning to extract significant representations from images of thin sections of lu-

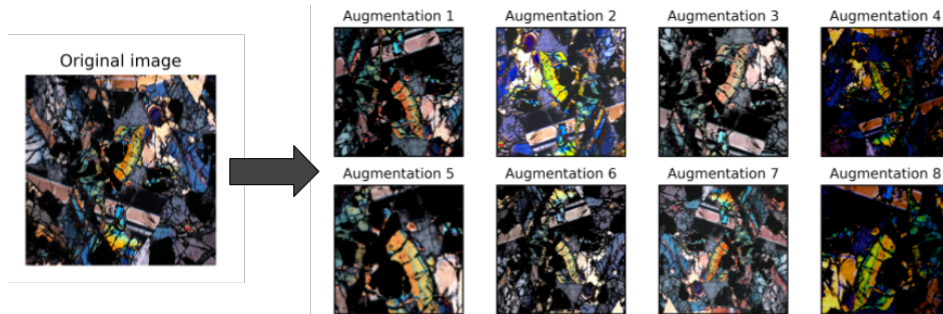


Figure 3: Example of augmentations of an image of a thin section of lunar rock.

nar rock. The implementation of contrastive learning will be utilized within a network consisting of a transfer model of convolutional residual connections and a classification head. Subsequently, the derived representations will serve as input for training a binary classifier. In the following sections, these fundamental concepts will be introduced in detail.

### 3.1. Transfer Learning with Inception Residual Networks

The introduction of residual connections accelerated the research on neural networks [29]. Residual connections enabled the training of deeper networks and the mitigation of the vanishing gradient problem by adding the input of the block to the transformation performed by the regular layers. This is achieved by incorporating identity mappings, allowing gradients to flow through the network more effectively during backpropagation and enhancing the model’s ability to learn complex features. ResNet is a convolutional neural architecture that vastly improved the accuracy of deep neural networks by implementing residual connections.

It was found that deeper convolutional networks with the inception principles proved effective in improving the use of computing resources within the network, hence improving the network while keeping computational resources constant [30]. Due to the success of both inception and ResNet networks, we choose to employ an Inception-ResNet-v2 [31] as the underlying transfer learning model, which is pre-trained on ImageNet.

Figure 4 shows the structure of the transfer learning model. The first 6 blocks depicted are a group of multiple layers (mostly convolutional) defined in [31]. After the first 6 layers are taken from the Inception-ResNet-v2 network, the network is equipped with classification heads, one for the SimCLR training and another for the binary classifier.



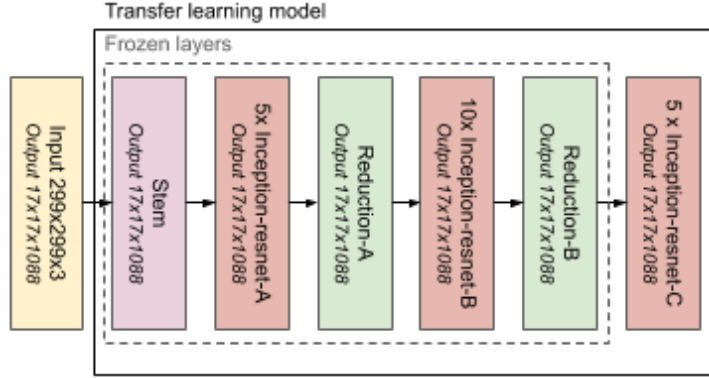


Figure 4: Customised Inception-ResNet-v2 adapted from [31]. 5 of the layers are frozen during network training and un-frozen during network fine-tuning.

### 3.2. Contrastive Learning with SimCLR

Contrastive learning methods, such as a Simple Framework for Contrastive Learning of Visual Representations (SimCLR) [32], have successfully learned generalisable features for various image tasks with limited data. SimCLR learns its general representations with the use of data augmentations. The process involves simultaneous optimisations of agreement among distinct transformations of the same image while minimizing concordance among transformations of dissimilar images. In this study, the neural network is trained using SimCLR. The SimCLR approach is in Figure 5. The input images  $x$  are augmented into two representations,  $\hat{x}_i$  and  $\hat{x}_j$ . Then, the representations are passed through the neural network, which is, in this paper, the Inception-ResNet-v2 network, resulting in the feature representations  $h_i$  and  $h_j$ . The feature representations are passed through a shallow and wide network,  $g(\cdot)$ , which then results in the final output of  $z_i$  and  $z_j$ . The loss function then maximizes the agreement between the two representations while minimizing the agreement between representations of other images. After the training is complete, the classification head  $g(\cdot)$  is removed, and the transfer model is fine-tuned according to the SimCLR approach and can be used for other classification or clustering tasks. The architecture of the network is in Figure 6.

### 3.3. Breccia/Basalt Binary Classifier

As in the contrastive learning training, the training of the breccia/basalt binary classifier is divided into two phases: The first phase freezes the transfer learning model and trains the classification head, and the second phase

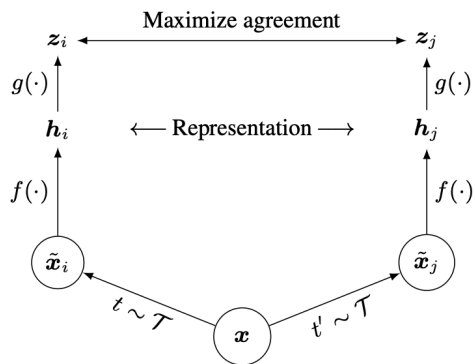


Figure 5: A simple framework for contrastive learning of visual representations from [32].

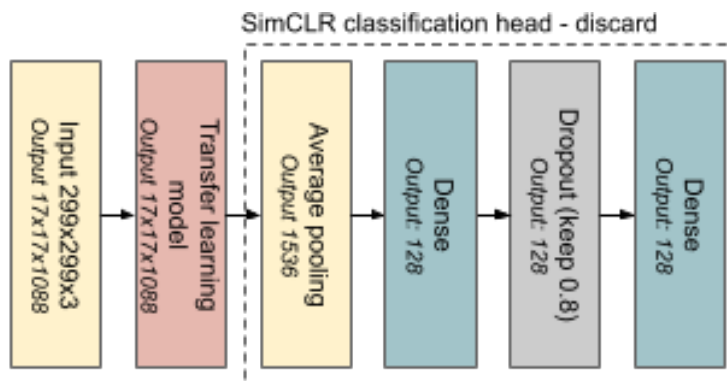


Figure 6: Architecture of the SimCLR training and fine-tuning of the transfer learning model. The four last blocks are the classification head, which is discarded after the fine-tuning of the transfer model is complete.

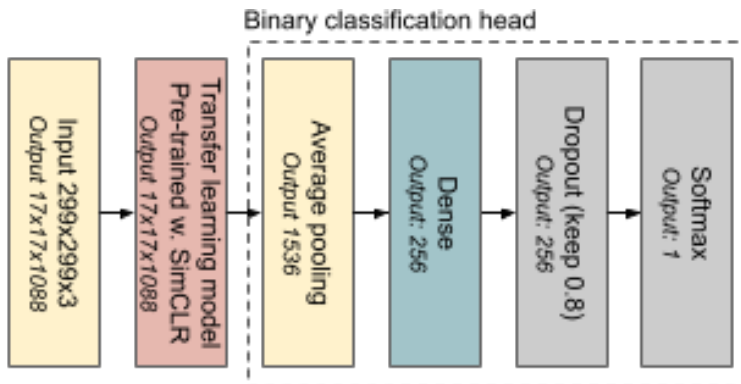


Figure 7: Architecture of the binary classifier. The transfer learning model Inception-ResNet-v2 is pre-trained with the SimCLR loss function and fine-tuned to the binary classifier.

fine-tunes the combined transfer model and classification head. The network is in Figure 7, where the transfer learning model is the same as in Figure 4 trained with the SimCLR approach.

During the first phase, the transfer learning model is frozen up till the second block of Inception-ResNet C, as it strikes a good balance between fine-tuning specialized features while not leading to a large entropic capacity and hence a strong tendency to overfit [33]. The Adaptive Moment Estimation (Adam) [34], with the AMSgrad version, is used, as it has been shown to be relatively more robust [35]. Though the learning rate is adaptive, the Adam optimizer is supplied with an initial learning rate of 0.001.

In the fine-tuning phase, the frozen layers are unfrozen. In this phase, a non-adaptive learning rate optimizer, Stochastic Gradient Descent (SGD), is used, with a low learning rate of 0.0001, to keep the updates small in the final tuning. Both phases are equipped with early stopping features [36] in order not to overtrain. To estimate the performance of the model, a stratified K-fold cross-validation was performed.

#### 4. Results

The SimCLR network was trained for at least 100 epochs, with the option of early stopping, since it has been observed that SimCLR benefits from extended training. Figure 8 illustrates the output of the final layer of Inception-ResNet-v2 trained with SimCLR, which represents the features that will be passed to the binary classifier. It effectively highlights various features, such as the shapes of minerals within a sample.

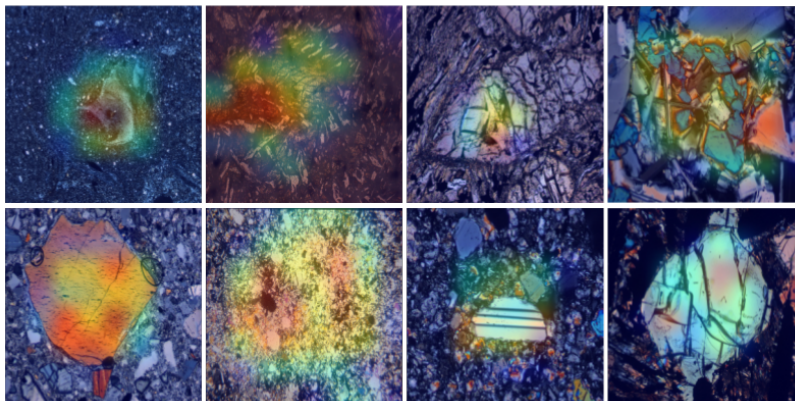


Figure 8: Example of activations of the SimCLR network on images of thin sections of lunar rock.

Since the samples have multiple pictures, the predictions of individual images can be grouped to predict the sample’s rock type, similar to the approach of ensemble learning. When the predictions for each sample are combined, it results in a better prediction, as is seen in Table 2. The resulting model proved successful, with an image accuracy of 93.51% ( $\pm 3.17$ ) and a group accuracy of 98.83% ( $\pm 0.95$ ), calculated on the test set. The results demonstrate that convolutional neural networks can effectively classify lunar rock types into their major categories.

## 5. Conclusion

In this study, we investigated the use of SimCLR, a contrastive learning method, for extracting features from lunar thin sections. The feature extraction was successful, as we were able to train a binary classifier using the extracted features from the dataset. The binary breccia/basalt classifier achieved an accuracy of 98.44% ( $\pm 1.47$ ). The classification task in this paper is relatively straightforward, as there are 513 samples total, and the classification is binary between basalt and breccia. An interesting prospect for future research would be to further categorize breccia into subgroups and include anorthosites in the analysis. While it may be challenging to segment minerals based solely on images without spectroscopy data, it would be intriguing to distinguish the samples into various subgroups of breccia based on grain sizes, such as fragmental breccias, glassy melt breccias, and impact-melt breccias.

The transfer model, fine-tuned with the SimCLR loss function, can be utilized as a transfer model for other analyses using the same dataset. This opens the possibility of continuing the research by employing the feature extraction network for segmentation and clustering approaches. Additionally, expanding the dataset would enhance the network’s effectiveness for other tasks.

## 6. Acknowledgements

We extend our sincere acknowledgements to the co-authors Victoria S. Engelschiøn, Piotr Knapczyk, Jonas Lewe, Clara Moriceau, and Romeo Haak. The research presented in this paper was done during their time as integral members of the Spaceship EAC group at the European Astronaut Centre, part of ESA. Acknowledgements to NASA and LPI for providing the vast dataset of images of the thin sections of lunar rocks.

## References

- [1] B. L. Jolliff, M. A. Wieczorek, C. K. Shearer, C. R. Neal, *New views of the Moon*, volume 60, Mineralogical Society of America Chantilly, 2006.
- [2] I. Crawford, M. Anand, C. Cockell, H. Falcke, D. Green, R. Jaumann, M. Wieczorek, *Back to the moon: The scientific rationale for resuming lunar surface exploration*, *Planetary and Space Science* 74 (2012) 3–14. URL: <https://www.sciencedirect.com/science/article/pii/S0032063312001444>. doi:<https://doi.org/10.1016/j.pss.2012.06.002>, scientific Preparations For Lunar Exploration.
- [3] G. H. Heiken, D. T. Vaniman, B. M. French, *Lunar sourcebook : a user’s guide to the moon*, 1991.
- [4] C. Meyer, *Lunar sample compendium* (2005).
- [5] J. H. Allton, *Catalog of apollo lunar surface geological sampling tools and containers*, NASA Lyndon B. Johnson Space Center, 1989.
- [6] University of Auckland, *Thin section microscopy*, 2024. URL: <https://www.geology.auckland.ac.nz/en/about/facilities/microscopy/thin-section-microscopy.html>, accessed: 07 October 2024.

- [7] T. Liu, Z. Liu, K. Zhang, C. Li, Y. Zhang, Z. Mu, M. Mu, M. Xu, Y. Zhang, X. Li, Research on the generation and annotation method of thin section images of tight oil reservoir based on deep learning, *Scientific Reports* 14 (2024) 12805.
- [8] S. J. Prince, *Understanding Deep Learning*, The MIT Press, 2023. URL: <http://udlbook.com>.
- [9] F. Sultana, A. Sufian, P. Dutta, Evolution of image segmentation using deep convolutional neural network: A survey, *CoRR* abs/2001.04074 (2020). URL: <https://arxiv.org/abs/2001.04074>. *arXiv:2001.04074*.
- [10] B. F. Windley, Anorthosites in the early crust of the earth and on the moon, *Nature* 226 (1970) 333–335.
- [11] J. A. Wood, A survey of lunar rock types and comparison of the crusts of earth and moon, in: *Sov.-Am. Conf. on the Cosmochem. of the Moon and Planets*, REPT-227, NASA, 1974.
- [12] L. S. P. E. Team, Preliminary examination of lunar samples from apollo 11: A physical, chemical, mineralogical, and biological analysis of 22 kilograms of lunar rocks and fines., *Science* 165 (1969) 1211–1227.
- [13] L. S. P. E. Team, Preliminary examination of lunar samples from apollo 12: A physical, chemical, mineralogical, and biological analysis of 34 kilograms of lunar rocks and fines, *Science* 167 (1970) 1325–1339.
- [14] D. Anderson, M. Bass, A. Bennett, D. Bogard, R. Brett, L. Bromwell, P. Butler Jr, W. Carrier III, R. Clark, T. Cobleigh, et al., Preliminary examination of lunar samples from apollo 14, *Science* 173 (1971) 681–693.
- [15] A. . P. E. Team, The apollo 15 lunar samples: A preliminary description, *Science* 175 (1972) 363–375.
- [16] A. . P. E. Team, The apollo 16 lunar samples: Petrographic and chemical description, *Science* 179 (1973) 23–34.
- [17] A. . P. E. Team, Apollo 17 lunar samples: Chemical and petrographic description, *Science* 182 (1973) 659–672.
- [18] H. H. Schmitt, *Lunar science a post-apollo view*, 1975.

- [19] F. Foucher, N. Bost, S. Janiec, A. Fonte, N. L. Breton, P. Perron, M. Bouquin, F. Lebas, M. Viso, P. Chazalnoël, F. Courtade, M. Villenave, F. Westall, Lithospace: An idea for an automated system for in situ petrographic thin section preparation on mars and other extraterrestrial rocky bodies, *Frontiers in Astronomy and Space Sciences* 8 (2021). doi:10.3389/fspas.2021.749494.
- [20] Cary, USGS photo F12653, USGS Open-File Report 2005-1190, Figure 034. Image file: </html1lib/btch545/btch545j/btch545z/pap00034.jpg> (accessed 25.04.2010), 1965. URL: </html1lib/btch545/btch545j/btch545z/pap00034.jpg>, uSGS Open-File Report 2005-1190.
- [21] R. A. Rubo, C. de Carvalho Carneiro, M. F. Michelon, R. dos Santos Gioria, Digital petrography: Mineralogy and porosity identification using machine learning algorithms in petrographic thin section images, *Journal of Petroleum Science and Engineering* 183 (2019) 106382. doi:10.1016/j.petrol.2019.106382.
- [22] T. Liu, C. Li, Z. Liu, K. Zhang, F. Liu, D. Li, Y. Zhang, Z. Liu, L. Liu, J. Huang, Research on image identification method of rock thin slices in tight oil reservoirs based on mask r-cnn, *Energies* 15 (2022) 5818. doi:10.3390/en15165818.
- [23] C. Guojian, L. Peisong, Rock thin-section image classification based on residual neural network, in: 2021 6th International Conference on Intelligent Computing and Signal Processing (ICSP), IEEE, 2021, pp. 521–524. doi:10.1109/ICSP51882.2021.9408983.
- [24] C. Su, S. jia Xu, K. yang Zhu, X. can Zhang, Rock classification in petrographic thin section images based on concatenated convolutional neural networks, 2020. URL: <https://arxiv.org/abs/2003.10437>. arXiv:2003.10437.
- [25] N. Aeronautics, S. A. (NASA), Apollo mission lunar sample photographs, Various. URL: [https://pdsimage2.wr.usgs.gov/Apollo/Lunar\\_Sample\\_Photos/](https://pdsimage2.wr.usgs.gov/Apollo/Lunar_Sample_Photos/), data available via the Planetary Data System (PDS3).
- [26] Lunar, P. I. (LPI), Lunar sample atlas: Apollo thin sections, Ongoing. URL: [https://www.lpi.usra.edu/lunar/samples/atlas/thin\\_sections/](https://www.lpi.usra.edu/lunar/samples/atlas/thin_sections/).

- [27] Lunar, N. J. S. C. Planetary Sciences Branch, Lunar sample and photo catalog curator, 2024. URL: <https://curator.jsc.nasa.gov/lunar/samplecatalog/index.cfm>.
- [28] L. Perez, J. Wang, The effectiveness of data augmentation in image classification using deep learning, CoRR abs/1712.04621 (2017). URL: <http://arxiv.org/abs/1712.04621>. arXiv:1712.04621.
- [29] K. He, X. Zhang, S. Ren, J. Sun, Deep residual learning for image recognition, 2015. URL: <https://arxiv.org/abs/1512.03385>. arXiv:1512.03385.
- [30] C. Szegedy, V. Vanhoucke, S. Ioffe, J. Shlens, Z. Wojna, Rethinking the inception architecture for computer vision, CoRR abs/1512.00567 (2015). URL: <http://arxiv.org/abs/1512.00567>. arXiv:1512.00567.
- [31] C. Szegedy, S. Ioffe, V. Vanhoucke, A. Alemi, Inception-v4, inception-resnet and the impact of residual connections on learning (2016). URL: <http://arxiv.org/abs/1602.07261>.
- [32] T. Chen, S. Kornblith, M. Norouzi, G. Hinton, A simple framework for contrastive learning of visual representations (2020). URL: <http://arxiv.org/abs/2002.05709>.
- [33] F. Chollet, Building powerful image classification models using very little data, 2016. URL: <https://blog.keras.io/building-powerful-image-classification-models-using-very-little-data.html>, accessed: 2024-08-15.
- [34] D. P. Kingma, J. Ba, Adam: A method for stochastic optimization, arXiv preprint arXiv:1412.6980 (2014).
- [35] S. J. Reddi, S. Kale, S. Kumar, On the convergence of adam and beyond, CoRR abs/1904.09237 (2019). URL: <http://arxiv.org/abs/1904.09237>. arXiv:1904.09237.
- [36] L. Prechelt, Early stopping-but when?, Neural Networks: Tricks of the trade (1998) 55–69.